


Calculated solar-neutrino capture rate for a radiochemical  $^{205}\text{Tl}$ -based solar-neutrino detectorJoel Kostensalo<sup>\*</sup> and Jouni Suhonen<sup>†</sup>*University of Jyväskylä, Department of Physics, P.O. Box 35, FI-40014, Finland*K. Zuber<sup>‡</sup>*Institute for Nuclear and Particle Physics, TU Dresden, 01069 Dresden, Germany* (Received 19 December 2019; revised manuscript received 22 January 2020; accepted 19 February 2020; published 4 March 2020)

Radiochemical experiments for low-energy solar-neutrino detection have been making headlines by exploiting the isotopes  $^{37}\text{Cl}$  and  $^{71}\text{Ga}$ . Such a very low-threshold measurement of this type can also be performed using  $^{205}\text{Tl}$ , which has been considered for decades for this purpose. A unique feature of this detector nucleus is the integration in the solar-neutrino flux over  $10^6$  of years owing to its long-living daughter  $^{205}\text{Pb}$ . In this Rapid Communication, we have calculated for the first time the cross section for the charged-current solar-neutrino scattering off  $^{205}\text{Tl}$ . Taking into account the solar-model-predicted neutrino fluxes and the electron-neutrino survival probabilities, a solar-neutrino capture rate of  $62.2 \pm 8.6$  solar-neutrino units is determined, a value significantly smaller than in previous estimates.

DOI: [10.1103/PhysRevC.101.031302](https://doi.org/10.1103/PhysRevC.101.031302)

*Introduction.* Neutrinos play a key role in several aspects of astroparticles and nuclear physics [1]. From the astrophysical point of view, solar neutrinos can be monitored in real-time measurements which allows to study neutrino properties, stellar structure, and evolution. To date, real-time monitoring of various neutrino chain reactions has been performed by the super-Kamiokande, the Sudbury Neutrino Observatory, KamLAND, and especially Borexino. Borexino was able to perform a common global fit of all the observed reactions of  $pp$ ,  $pep$ ,  $^7\text{Be}$ , and  $^8\text{B}$  in one detector [2].

An alternative method to the above-mentioned ones, used by the first solar-neutrino experiments, are the radio-chemical observations. These experiments employ the charged-current neutrino-nucleus scattering reaction,

$$\nu_e + (A, Z) \rightarrow e^- + (A, Z + 1) \quad (1)$$

for solar-neutrino detection. This reaction has been used in the pioneering Homestake experiment using  $^{37}\text{Cl}$  as the detector material [3], and, in this experiment, a deficit with respect to expectation was found. First measurements of the fundamental  $pp$  neutrinos were based on  $^{71}\text{Ga}$  (GALLEX, GNO, and SAGE). Several other nuclides, with different reaction thresholds, have been considered for more refined overall spectral analyses [4]. A very interesting candidate of this type is  $^{205}\text{Tl}$ , which has a very low threshold for solar neutrinos.

*The  $^{205}\text{Tl}$  reaction.* The dominant charged-current neutrino-nucleus reaction under discussion is

$$^{205}\text{Tl}(1/2^+) + \nu_e \rightarrow ^{205}\text{Pb}(1/2^-) + e^-, \quad (2)$$

which feeds the first excited state of  $^{205}\text{Pb}$  at 2.33 keV and is of first-forbidden nonunique type [5]. Only a tiny portion of the feeding goes to the  $5/2^-$  ground state of  $^{205}\text{Pb}$ , the corresponding transition being first-forbidden unique [5,6]. According to the current atomic mass evaluation [7], the  $Q$  value is given by  $50.6 \pm 0.5$  keV, which is so far the lowest threshold among radiochemical approaches for solar-neutrino detection. This results in a total threshold of about 53 keV for the transition (2). Furthermore, a unique feature of this reaction is the possibility for long-term monitoring of the average solar-neutrino flux and, hence, the mean solar luminosity over the past  $4.31 \times 10^6$  yr due to the long half-life of  $1.73(7) \times 10^7$  yr of  $^{205}\text{Pb}$  [8]. Hence, such a measurement could shed light on the long-term stability of the Sun and, therefore, on the stability of stars, in general [4].

The first studies of the Tl experiment were performed by Refs. [9–12] which later became the LOREX experiment [13,14]. Although several experimental aspects have already been addressed or have been worked on, the major remaining uncertainty is the cross section for this reaction. Hence, it is essential to get a reliable estimate of this cross section and this Rapid Communication reports on the calculation of this important quantity using current state-of-the-art techniques.

*Calculation of the  $^{205}\text{Tl}$  cross section.* The calculations for the neutrino-nucleus cross section are based on the O'Connell *et al.* [15] and Donnelly and Peccei [16] method for the treatment of semileptonic processes in nuclei. Details of the formalism as it is applied here can be found from Ref. [17]. A streamlined version has also been given in the recent papers [18,19].

The nuclear-structure calculations were performed in the shell-model framework using the shell-model code NUSHELLX@MSU [20] with the Hamiltonian *khhe* [21] in

<sup>\*</sup>joel.j.kostensalo@student.jyu.fi<sup>†</sup>jouni.t.suhonen@jyu.fi<sup>‡</sup>zuber@physik.tu-dresden.de

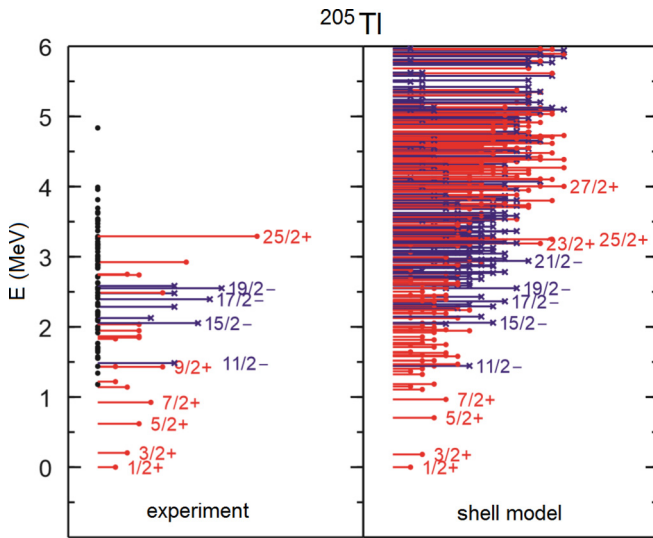


FIG. 1. Experimental and shell-model excitation spectra for  $^{205}\text{Tl}$ . Each horizontal bar represents a nuclear state, and its length is proportional to the angular momentum of the state.

the complete valence space spanned by the proton orbitals  $0g_{7/2}$ ,  $1d$ ,  $2s$ , and  $0h_{11/2}$ , and the neutron orbitals  $0h_{9/2}$ ,  $1f$ ,  $2p$ , and  $0i_{13/2}$ . As can be seen from Figs. 1 and 2, the energy spectra of the relevant nuclei are reproduced astonishingly well. The nucleus  $^{205}\text{Pb}$  decays via the  $^{205}\text{Pb}(5/2^-) \rightarrow ^{205}\text{Tl}(1/2^+)$  ground-state-to-ground-state  $\beta$  transition, and the corresponding half-life can be reproduced when  $g_A = 0.75$  is adopted as the effective axial-vector coupling. This result is consistent with the previous calculations for  $\beta$  decays in heavy nuclei [22]. However, as shown in Fig. 3 for the computed scattering cross section, the leading contributions come from the  $0^-$ ,  $1^-$ , and  $2^-$  multipole transitions. At the zero-momentum-transfer limit, these correspond

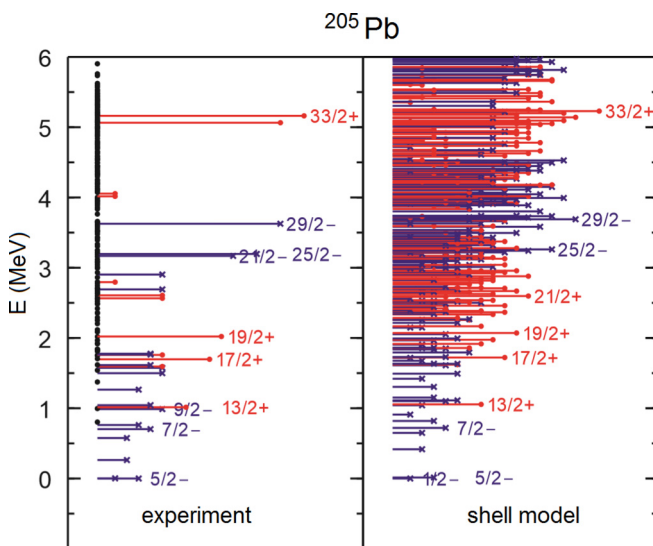


FIG. 2. Experimental and shell-model excitation spectra for  $^{205}\text{Pb}$ . Each horizontal bar represents a nuclear state, and its length is proportional to the angular momentum of the state.

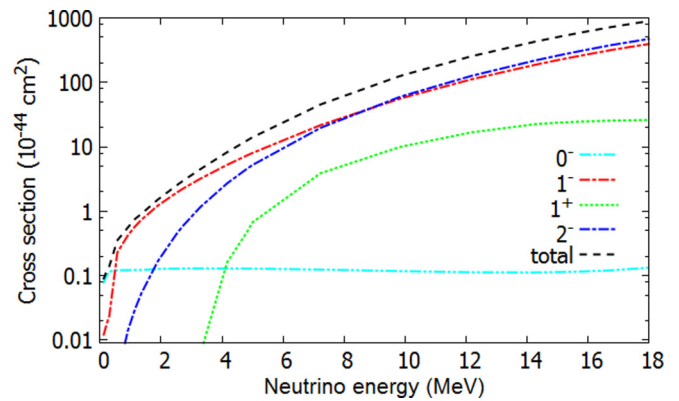


FIG. 3. Capture cross section for neutrino capture on  $^{205}\text{Tl}$  as function of neutrino energy for the leading transition multipoles with  $g_A = 1.00$ .

to the spin-dipole type of  $\beta$  transitions discussed extensively, e.g., in Refs. [23–25]. In the nuclear mass regions relevant to the above decay transition, which is a tensor transition, the effective values  $g_A \approx 0.90$  [23] and  $g_A \approx 0.5$  [25] have been obtained. Thus, the presently obtained effective value resides in the middle of these values. Furthermore, in the works [23–25], values of  $g_A \approx 0.38$ – $0.97$  were obtained for the  $1^-$  type of spin-dipole transitions, and values of  $g_A \approx 0.66$ – $0.92$  were obtained for the  $0^-$  type of spin-dipole transitions. This means that there is a lot of variation in the obtained values of the effective  $g_A$  for the spin-dipole type of  $\beta$  transitions. It is also not so clear how these values propagate to values of  $g_A$  for finite momentum transfers involved in the neutrino-nucleus scattering. Based on the above, we have taken the conservative approach and estimate the uncertainties related to nuclear structure by considering here the range of  $g_A = 0.75$ – $1.00$  for all transitions: a range which covers a reasonable range of values adopted in the above works and other large-scale shell-model calculations.

Since the exact energy of the low-lying states plays a significant role in determining the cross section for neutrinos with low energies, such as  $pp$  neutrinos, the energies of the dominating low-lying states were adjusted to their experimental values. The energy-adjusted states were the lowest two  $1/2^-$  states and the lowest three  $3/2^-$  and  $1/2^+$  states. Based on the ordering of the levels in the shell-model calculation, the state at 803 keV was taken to be  $1/2^-$  and the state at 996 keV was taken to be  $3/2^-$ .

The contributions by multipolarity of the transition operators are shown in Fig. 3 and by individual states in Fig. 4. The ground state of  $^{205}\text{Tl}$  has the spin-parity  $1/2^+$  so that the Gamow-Teller type of transitions ( $1^+$  transition multipole) are possible only to  $1/2^+$  and  $3/2^+$  states in  $^{205}\text{Pb}$ . There are only three known  $1/2^+$  states in  $^{205}\text{Pb}$  at 2795, 4016, and 4055 keV and no known  $3/2^+$  states. Gamow-Teller transitions are, therefore, available only for  $^8\text{B}$  and  $hep$  neutrinos, which happen to have relatively low fluxes in the standard solar models [26]. For these higher-energy neutrinos, the  $1/2^+$  state at 4016 keV gives a noticeable contribution. However, the numerous low-lying negative-parity states still dominate even at the higher neutrino energies as the transitions to the low-lying

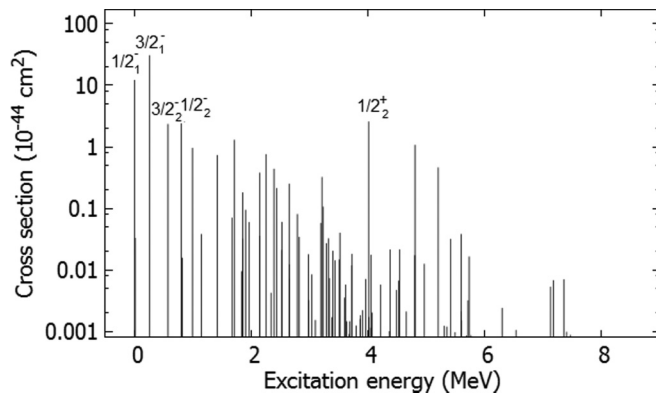


FIG. 4. Contributions of the individual states to the  ${}^8\text{B}$  neutrino cross section with  $g_A = 1.00$ . The horizontal axis gives the excitation energy in  ${}^{205}\text{Pb}$ .

states have a significant energy advantage. Due to this lack of positive-parity states with small angular momenta, the cross section is dominated by the spin-dipole type of forbidden transitions which render the total cross section smaller than expected from energy arguments alone.

The energy dependence of the scattering cross section for different transition multipoles is highly nontrivial, which is exemplified by the behavior of the  $0^-$  multipole. Based on our calculations, there is a significant contribution to this multipole from the transition to the first  $1/2^-$  state, but the other states contribute very little. Due to the first  $1/2^-$  contribution the cross section for the  $0^-$  multipole rises qualitatively in a similar way as that for the other multipoles up to about 0.4 MeV in neutrino energy but is mostly flat in the 0.5–15-MeV range. The reason for the flatness is due to the fact that the cross section is proportional to  $p_e E_e F(Z)$  (see, e.g., Ref. [27]), where  $p_e$  is the momentum of the outgoing electron,  $E_e$  is the total energy of the electron, and  $F(Z)$  is the Fermi function taking into account the final-state Coulomb interaction. The Fermi function is very large for the low energies, which is counterbalanced by the small  $p_e$  and  $E_e$ . For higher neutrino energies (which are not of interest here), we end up with the product  $p_e E_e$  dominating, leading to an approximately quadratic energy dependence of the cross section. For the other transition multipoles, there are a large number of important low-energy nuclear final states to scatter to, which is why the corresponding cross sections grow much faster at the low neutrino energies.

*Reaction rates in solar-neutrino units.* Owing to the small cross section of low-energy neutrino-nucleus interactions, it is convenient to present the neutrino-capture rate in the solar-neutrino units (SNU), given as 1 SNU =  $10^{-36}$  capture reactions per target atom per second. Then, the neutrino-capture rate  $R$  is described by

$$R = 10^{36} \sum_i \int \sigma(E) \phi_i(E) dE, \quad (3)$$

where  $E$ ,  $\sigma(E)$ , and  $\phi_i(E)$  are the neutrino energy, the neutrino-capture cross section (see the previous section), and the differential neutrino spectra. The latter are given at a distance of 1 AU. The sum in Eq. (3) includes all eight neutrino components from the  $pp$  and carbon nitrogen oxygen cycles.

For the calculation of solar-neutrino capture rates, the fluxes of the solar model BS05(OP) were adopted (see Table 2 in Ref. [26]) with the neutrino spectrum shapes available on Bahcall's website [28]. With these spectra and fluxes, we get for the capture rate 100.2 SNU with  $g_A = 0.75$  and 132.4 SNU with  $g_A = 1.00$  when the survival probability of electron neutrinos is not taken into account. Since the majority of the cross section comes from  $1^-$  and  $2^-$  types of transitions, the  $g_A$  dependence is not the trivial  $g_A^2$  as both the vector and the axial-vector components contribute. With the electron-neutrino survival probability of 0.54 for the  $pp$ ,  ${}^7\text{Be}$ , and  ${}^{13}\text{N}$  neutrinos, and 0.50 for the  $pep$ ,  ${}^{15}\text{O}$ , and  ${}^{17}\text{F}$  neutrinos, and 0.36 for the  ${}^8\text{B}$  neutrinos [29], we end up with a result of

$$R({}^{205}\text{Tl}) = 62.2 \pm 8.6 \text{ SNU} \quad (4)$$

for the capture rate.

*Summary and conclusions.* Given the revived interest in solar-neutrino detection using  ${}^{205}\text{Tl}$  due to its very small energy threshold, we have performed a large-scale shell-model calculation to find out the cross section for the conversion of  ${}^{205}\text{Tl}$  to  ${}^{205}\text{Pb}$ . Combined with the neutrino fluxes predicted by established solar models and taking into account the survival probabilities of electron neutrinos, the capture rate turns out to be  $62.2 \pm 8.6$  SNU. This capture rate is significantly smaller than anticipated by previous estimations.

*Acknowledgments.* The authors would like to thank Dr. Y. Litvinov for bringing this issue to our attention. This work has been partially supported by the Academy of Finland under Academy Project No. 318043. J.K. acknowledges financial support from the Jenny and Antti Wihuri Foundation.

[1] H. Ejiri, J. Suhonen, and K. Zuber, *Phys. Rep.* **797**, 1 (2019).  
 [2] G. M. Agostini *et al.*, *Phys. Rev. D* **100**, 082004 (2018).  
 [3] B. T. Cleveland *et al.*, *Astrophys. J.* **496**, 505 (1998).  
 [4] J. N. Bahcall, *Neutrino Astrophysics* (Cambridge University Press, Cambridge, UK, 1989).  
 [5] J. Kostensalo and J. Suhonen, *Phys. Lett. B* **781**, 480 (2018).  
 [6] J. Suhonen, *From Nucleons to Nucleus: Concepts of Microscopic Nuclear Theory* (Springer, Berlin, 2007).  
 [7] M. Wang, G. Audi, F. G. Kondev, W. J. Huang, S. Naimi, and X. Xu, *Chin. Phys. C* **41**, 030003 (2017).

[8] F. G. Kondev, *Nucl. Data Sheets* **101**, 521 (2004).  
 [9] S. M. Freedman *et al.*, *Science* **193**, 1117 (1976).  
 [10] S. M. Freedman *et al.*, *Nucl. Instrum. Methods Phys. Res., Sect. A* **271**, 267 (1988).  
 [11] P. Kienle, *Nucl. Instrum. Methods Phys. Res., Sect. A* **271**, 277 (1988).  
 [12] W. Henning and D. Schuell, *Nucl. Instrum. Methods Phys. Res., Sect. A* **271**, 324 (1988).  
 [13] M. K. Pavicevic, *Nucl. Instrum. Methods Phys. Res., Sect. A* **271**, 287 (1988).

- [14] M. K. Pavićević *et al.*, *Adv. High Energy Phys.* **2012**, 274614 (2012).
- [15] J. S. O'Connell, T. W. Donnelly, and J. D. Walecka, *Phys. Rev. C* **6**, 719 (1972).
- [16] T. W. Donnelly and R. D. Peccei, *Phys. Rep.* **50**, 1 (1979).
- [17] E. Ydrefors and J. Suhonen, *Adv. High Energy Phys.* **2012**, 373946 (2012).
- [18] J. Kostensalo, J. Suhonen, and K. Zuber, *Phys. Rev. C* **97**, 034309 (2018).
- [19] J. Kostensalo, J. Suhonen, C. Giunti, and P. C. Srivastava, *Phys. Lett. B* **795**, 542 (2019).
- [20] B. A. Brown and W. D. M. Rae, *Nucl. Data Sheets* **120**, 115 (2014).
- [21] E. K. Warburton and B. A. Brown, *Phys. Rev. C* **43**, 602 (1991).
- [22] J. Suhonen, *Front. Phys.* **5**, 55 (2017).
- [23] E. K. Warburton, *Phys. Rev. C* **42**, 2479 (1990).
- [24] E. K. Warburton, *Phys. Rev. C* **44**, 233 (1991).
- [25] Q. Zhi, E. Caurier, J. J. Cuenca-García, K. Langanke, G. Martínez-Pinedo, and K. Sieja, *Phys. Rev. C* **87**, 025803 (2013).
- [26] J. N. Bahcall *et al.*, *Astrophys. J., Lett.* **621**, L85 (2005).
- [27] H. Ejiri and S. R. Elliott, *Phys. Rev. C* **89**, 055501 (2014).
- [28] J. N. Bahcall, Software and data for solar neutrino research [<http://www.sns.ias.edu/jnb/>]
- [29] M. Agostini *et al.* (The Borexino Collaboration), *Nature (London)* **562**, 505 (2018).